Journal of Multiscale Modelling
Vol. 3, Nos. 1 & 2 (2011) 91–107

DOI: 10.1142/S1756973711000376

Imperial College Press
www.icpress.co.uk

AN ADVANCED ADAPTIVE FINITE ELEMENT CODE APPLIED FOR COATING-SUBSTRATE SIMULATION

JÜRGEN LEOPOLD*,‡, KATRIN HELLER*,
ARNDT MEYER† and REINER WOHLGEMUTH*

*TBZ-PARIV GmbH, Bernsdorfer Straße 210-212
D-09126 Chemnitz, Germany

†Chemnitz University of Technology, Faculty of Mathematics
Chair of Numerical Analysis, Reichenhainer Straße 41
D-09126 Chemnitz, Germany
‡jleopold@tbz-pariv.de

The stability of coating-substrate systems influences the chip formation and the surface integrity of the new generated workpiece surface, too. Using finite element (FE) simulation, deformations, strains and stresses in coated tools, caused by external and internal loads, can be computed on a microscopic scale. Since both, the whole macroscopic tool (in mm-scale) and the microscopic coating layers (in μm-scale up to nm-scale) must be included in the same geometrical simulation model, graded high-resolution FE meshes must be used. Nevertheless, the number of nodes in the 3D computational FE grid reaches some millions, leading to large computational time and storage requirements. For this reason, an advanced adaptive finite element (AAFEM) software has been developed and used for the simulation.

Keywords: Coating-substrate systems; finite element method; superlattice coatings.

1. Introduction

To increase the performance of cutting tools, substrate materials, cutting tool microgeometry and also the cutting conditions have continually been improved. In recent years, an increase in efficiency of the overall cutting process has been reached by a lot of different coating-substrate-systems on tools. Coated tools have a higher edge life compared to uncoated ones,[1] can produce a higher surface quality of the new detail,[2] and are well suited for high-speed, dry and micro machining. So coating technology gained a growing importance for industrial applications. Nowadays more than three-quarters of all tools are coated with several materials and coating systems. Recently, manufacturers of coated tools have had a lot of experience and knowledge about coating technology and well-suited material combinations for selected industrial applications available but do not integrate numerical methods for investigating the mechanical properties of coating systems.[3] Coating optimization is still mostly achieved by means of "more or less inspired" trial and error approaches,[4]

and the development of new coating systems, especially for new advanced machining technologies, requires a series of expensive experiments,[5] in which the suitability of the coated tool for the technological process, its resistance against mechanical and thermal loads and the adhesion between the different materials must be investigated, since the adhesion of substrate and coating(s) has special importance for the further optimization of coating technology.[6]

New workpiece materials, like nickel basic alloys or titanium, and also the protection of the environment by dry machining put in a claim for new advanced coating-substrate-systems. New cutting tools with improved properties for dry machining have been developed.[7] Whereas abrasion is one of the main wear mechanisms in wet machining, the avoidance of cooling lubricants leads to increase the adhesive forces in dry cutting processes. Due to high temperatures in dry machining the chips and the workpiece material become higher plastic deformations. This is the reason, why there is a strong adherence between the cutting tool on one hand site and the workpiece material on the other hand. That increases the shear stresses in the subsurface layers of the tool. Several properties of the coating-substrate system are required to achieve a high wear resistance as well as a high process safety in cutting.[8] The substrate determines geometry, stiffness and high strength, whereas the tribological properties and the thermal and diffusion barrier depends on the coating properties (Fig. 1).

The intermediate zone between coating and substrate is called interface and determines the film adhesion. The interface strength can be increased by using mechanical substrate treatment.[9] Requirements on coatings for wear protection for

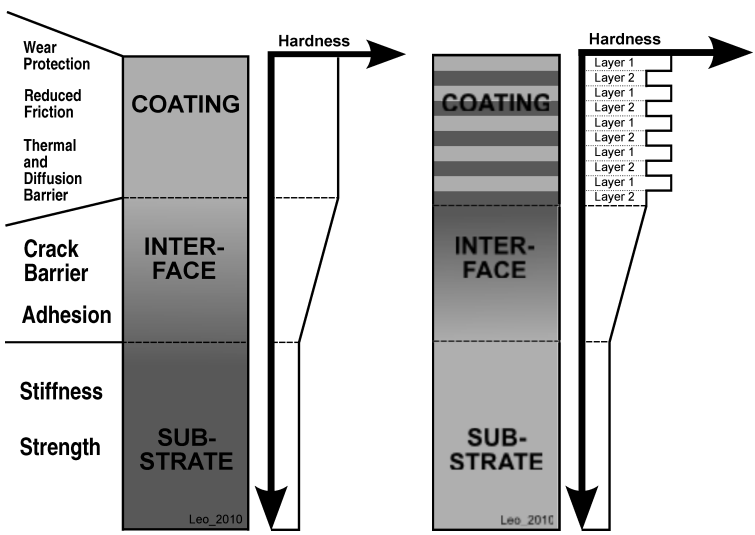

Fig. 1. Requirements on coating-substrate systems (a) standard coating and (b) superlattice coating.

cutting of new materials are a high hardness compared with a sufficient stiffness. In addition, reduced tribological interactions to the workpiece material have to be achieved at the surface of the coating. Typically mono- or few multilayer coatings [Fig. 1(a)] like TiN, TiCN, TiAlN, CrN or DLC use thickness between 1 μm and 10 μm. It was found out, that hard materials (e.g., TiN, Al_2O_3) are used successfully as coatings to increase tool life by a factor of 4–20. For superlattice coatings, commonly be used in machining of new materials and dry manufacturing [Fig. 1(b)], the thickness of one layer is typically less than 100 nm. One example is given in Fig. 2 from Ref. 10.

Yang and Zhao[11] found out that the highest hardness exists for a single layer thickness of 7.5 nm and a (200) orientation. Very important coating combinations concerning the research and development and industrial applications are given in Fig. 3. TiN/CrN is one of the most important ones and will be highlighted in this paper.

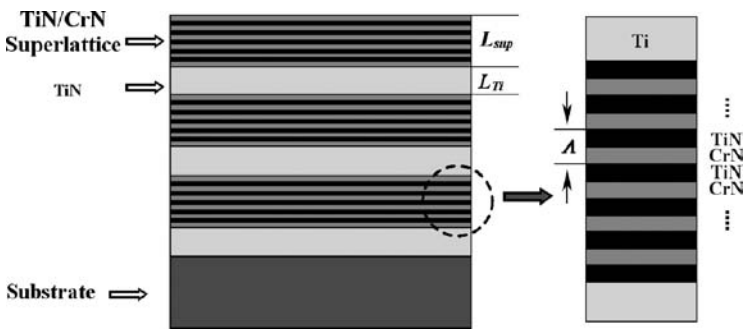

Fig. 2. Schematic diagram of the multilayered coatings with alternate pure Ti layers and TiN/CrN superlattices.

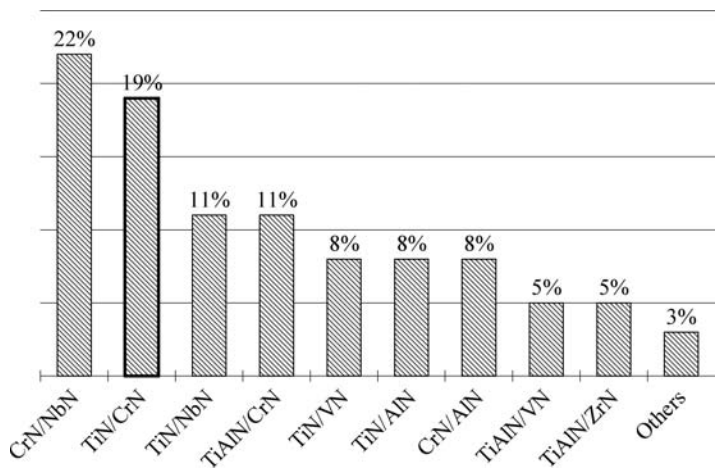

Fig. 3. Overview to superlattice coatings.

Table 1. Theoretically methods to investigate coating-substrate systems.

Numerical methods	Analytical methods
Numerically simulation by Landau–Khatalnikov-Theory (Ref. 12)	Small angle X-ray diffraction (SAXRD) (Ref. 19)
Mean-field theory (Ref. 13)	Molecular dynamics (Ref. 20)
Monte-Carlo-simulation (Ref. 13)	
Discrete dislocation dynamics (Ref. 14) (DDD)	
Finite element method (Refs. 15–18)	

Experimental trial-and-error-methods are applied to optimize the coating substrate system in the industry. This takes a lot of time and causes high costs. Since some years, theoretically methods are developed to reduce the time-to-market process in the metal cutting industry based on research, development and application of new coating-substrate systems. Table 1 summarizes typical theoretical methods.

The finite element method (FEM) was applied in previous investigations to coating-substrate systems with a layer thickness of more than 1 μm. Based on a 2D-ANSYS®-model, the adhesive strength between substrate and a thin film was calculated in Ref. 15. A new FEM-code, suitable for parallel computer systems with an arbitrary number of processors, has been developed and tested on different coating-substrate systems by Leopold, Meisel, Wohlgemuth and Liebich.[16] The 3D FEM discretization of the coated tool reaches more than 800,000 elements with approximately 2,500,000 unknowns. In that way, deformations and stresses caused by external loads have been calculated on a microscopic scale with sufficient accuracy and detail resolution. Nowadays a 2D-ABAQUS®-model with about 34,505 nodes and 10,428 elements was applied to simulate thermally induced residual stresses developed in a plate of brittle thermal barrier coatings on ductile substrates.[18] Up to now, FEM has not been applied to investigate superlattice coatings. The focus of this paper is to investigate TiN/CrN superlattice coating-substrate systems with a new developed advanced adaptive FEM (AAFEM) code.

2. Modeling of Superlattice Coatings by AAFEM

2.1. *Basics of AAFEM*

The AAFEM is developed constantly. It contains many features, which are advanced in comparison with other better known software. These features are:

- Adaptive mesh refinement:
  - strong reduction of elements and nodes
  - high accurate solutions with low calculation times
- Facility for superlattice simulation by FEM
- The software module is free for members of the consortium and can be used for investigations within the M3-2S project.

2.1.1. *Partial differential equations to be approximated*

The principles of the FEM will not be discussed in detail. A good overview is given in Refs. 21 and 22. The AAFEM is an FEM-Software,[23–25] which is concerned to solve the following partial differential equations (p.d.e.'s) approximately.

(1) Potential/reaction-diffusion problem (NDOF = 1)

$$\begin{aligned} -\mathrm{div}(A(\mathbf{x})\nabla u) + \gamma(\mathbf{x})u &= f(\mathbf{x}) \quad && \text{in } \Omega \\ u &= g_D && \text{on } \Gamma_D \\ \mathbf{n} \cdot A(\mathbf{x})\nabla u &= g_N && \text{on } \Gamma_N \end{aligned} \tag{1}$$

with given $f(\mathbf{x}), A(\mathbf{x}) = \mathrm{diag}(\alpha_1(\mathbf{x}), \alpha_2(\mathbf{x}))$ and $\gamma(\mathbf{x}) \geq 0$ (constant in subdomains of $\Omega \subset \mathbb{R}$).

(2) Lamé equation of linear elasticity (NDOF = 2) with given $f(\mathbf{x})$, Young's modulus $E(\mathbf{x})$ and Poissons ratio $\nu(\mathbf{x})$ (constant in subdomains of $\Omega \subset \mathbb{R}$).

In both cases we use Cartesian (x, y)-coordinates or cylindrical (r, z)-coordinates. The Lamé equation is so given in its weak formulation only.

2.1.2. *Boundary conditions (b.c.'s)*

We define $\partial\Omega = \Gamma_D \cup \Gamma_N$, with $\Gamma_D \cup \Gamma_N = \emptyset$.

(i) The Dirichlet b.c.'s on Γ_D cut into two types. In both cases we define $u = g_D(x)$

(1) In the first case $g_D(x)$ can be a quadratic function prescribed by 3 values: $g_D(N_A)$, $g_D(N_E)$ and $g_D(N_M)$
(N_A and N_E are endpoints of the edge E; N_M is the midpoint of E)

(2) In the second case $g_D(x)$ is a vector function. We can prescribe

(a) a "slip-condition". That means that $\mathbf{u} \cdot \mathbf{n} = 0$ (normally to the edge-vector $\mathbf{E} : \mathbf{E} \cdot \mathbf{n} = 0$)

(b) or a contact condition. $\mathbf{x} + \mathbf{u}(\mathbf{x})$ shall not penetrate an obstacle $\{\mathbf{p} + \lambda\mathbf{t} : \lambda \in \mathbb{R}\}$, with given $\mathbf{p}$ and $\mathbf{t} \Rightarrow \mathbf{u} \cdot \mathbf{n} \geq (\mathbf{p} - \mathbf{x}) \cdot \mathbf{n}$.

(ii) Even we have two types of Neumann b.c.'s on $\Gamma_N = \Gamma_{N,i} \cup \Gamma_{N,0}$. On $\Gamma_{N,i}$ the b.c.'s are prescribed from the input file. On the remaining part $\Gamma_{N,0}$ homogeneous b.c.'s are taken automatically. We define a $g_N(x)$ as follows:

(1) $g_N(x) = \mathbf{n} \cdot (A(x)\nabla u)$ on E. $g_N(x)$ is again a quadratic function on E from the given endpoints $g_N(N_A)$ and $g_N(N_E)$ and the midpoint $g_N(N_M)$

(2) in second case tractions $\mathbf{g}_N(X)$ on E are prescribed
$\mathbf{g}_N(x) = B_0(\mathbf{n})^T(C \cdot B_\rho(\nabla)u)$. $\mathbf{g}_N(x)$ are possibly quadratic on E.

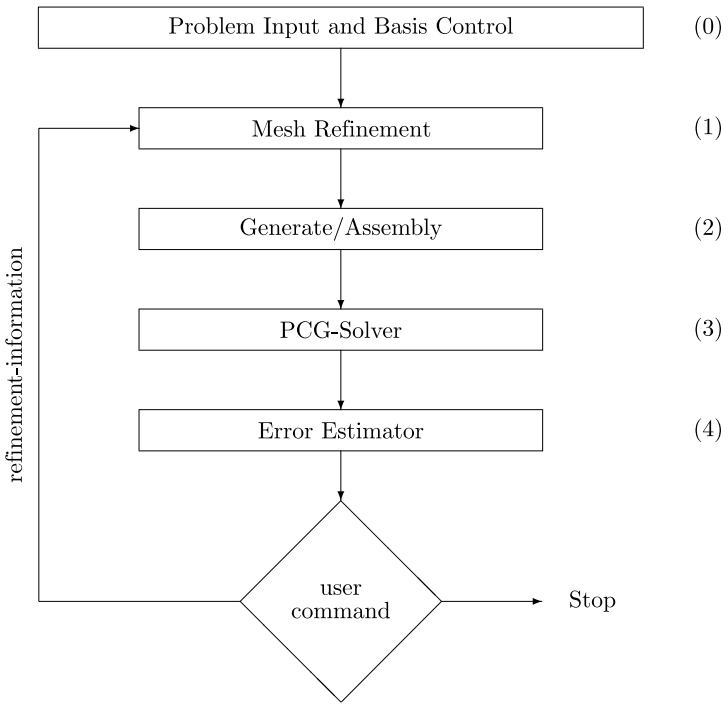

Fig. 4. Flow chart of AAFEM.

2.2. *Handling AAFEM Software*

2.2.1. *General program structure of AAFEM*

The general run overview of AAFEM is given in Fig. 4. The five main steps [(0)–(4)] are presented in the following section.

Postprocessing and grafic proceed at position "user command". At this point refinement-informations (refinement of all elements, auto refinement, recomputation without mesh-refinement, etc.) can be committed to the program.

2.2.2. *Description of main-steps*

Problem input — Step (0) That step is related to the definition of the problem: The two problems (1) and (2) from Sec. 2.1.1 and reading the coarse mesh with triangles or quadrilaterals cause four cases:

- "mesh 31": [triangular elements, problem (1)]
- "mesh 32": [triangular elements, problem (2)]
- "mesh 41": [quadrilateral elements, problem (1)]
- "mesh 42": [quadrilateral elements, problem (2)]

Additionally we have to input element control (linear or quadratic) and refinement strategy (compare Sec. 2.3.1)

- In the triangular case:
  "g" ... Bänsch-Green
  "r" ... Red-Green
  "h" ... Red with hanging nodes
- In the quadrilateral case:
  hanging nodes are always used, aspect ratio is selectable

Mesh refinement — Step (1) Due to input informations on the elements and/or edges and due to local properties of each element (aspect ratio, some subdivided edges) the elements are subdivided into 2 or 4 smaller elements by changing the three data structures (more nodes/edges/elements). This is repeated until there is no more reason for subdividing.

Generate/Assembly — Step (2) That step defines the stiffness-matrix and right-hand side for approximating the p.d.e. on the actual mesh.

PCG-Solver — Step (3) If there belong Nn nodes in actual mesh, we have to solve $p = Nn \cdot NDof$ as Dimension of the linear system $K\mathbf{u} = \mathbf{b}$. The number of unknowns is smaller due to some given types of Dirichlet b.c.'s or due to the fact of having hanging nodes. The improvement of the existing problem follows by preconditioning. So we have to solve the linear system $P^T K\mathbf{u} = P^T\mathbf{b}$. The projector P is adjustable inside the program structure.

Error-Estimator — Step (4) This is the most important step for the basic control of the adaptive meshing. η_E is the edge oriented error estimator. It is calculated over all elements and we take $\eta = \max_{\forall E} \eta_E$ and mark all edges E for subdivisions, if $\eta_E^2 \geq \tau_{\text{Tol}} \cdot \eta^2$ (at first $\tau_{\text{Tol}} = 0.8$).

If the number of marked edges is too low ($\leq 10\%$ of all edges), we define new $\tau_{\text{Tol}} = 0.5\tau_{\text{Tol}}$.

For an overview of known error estimators see Refs. 26 and 27 and the references therein.

2.3. *Extension of AAFEM for superlattice-coatings*

2.3.1. *The adaptive strategy*

The marked elements from the main step (4) in Sec. 2.2.2 are subdivided into smaller parts due to some strategies.

There are two basic strategies for subdividing in the case of 2D calculations and triangular meshes:

- The so-called "red" subdivision of a triangle into four sub-triangles of equal shape and size (see Fig. 5) and
- The so-called "green" subdivision into two parts (see Fig. 6).

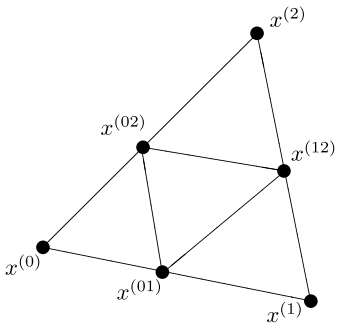

Fig. 5. Red subdivision.

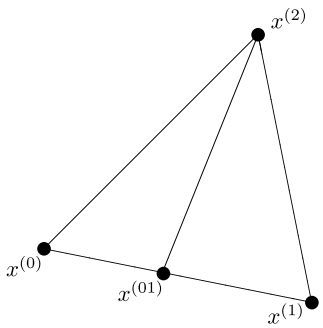

Fig. 6. Green subdivision.

We have got at least three strategies for the whole mesh.

The strategy "Bänsch–Green"[28] uses green subdivisions only. If we start with the red subdivision on all marked triangles we can continue with two possible sub-strategies:

"**Red-Green**" We produce a conforming FE mesh by adding green subdivisions on triangles with at least one subdivided edge. (These green elements are removed before deeper subdividing in the next step.)

"**Red with hanging nodes**" No additional subdivision on elements with one subdivided edge — we accept a nonconforming mesh with so-called "hanging nodes". The solver can guarantee that we work in the conforming subspace, i.e., we use continuous FE functions (see Ref. 29).

In the quadrilateral case similar ideas have been used. The most simple strategy in the mesh handling is again "red-hanging nodes", i.e., subdividing of each marked element into four parts and permitting of maximal two hanging nodes on two non-opposite sides. This is simply generalized into 3D, whereas the generalization of the "red" triangular case leads to a new property. The resulting sub-tetrahedrons are of the same volume but not of the same shape.

An important fact for the following considerations is the definition of the vertices of the son-elements. In the triangular case the new nodes are calculated first from the formula

$$x^{\text{son}} := \frac{1}{2}\left(x^{\text{father1}} + x^{\text{father2}}\right) \tag{2}$$

is then used for defining the new sub-edges. If this technique is repeated a couple of times neighboring nodes coincide in more and more leading digits. More precisely, a node x^{son} generated at an Lth level subdivision of some coarse element coincides with its two fathers in about L leading digits (in their binary representation). That means, the coordinates itself are correct until machine accuracy, but differences of neighboring nodes lead to cancellations of about L digits. In classical FE codes with uniform mesh refinement this played no role, because L was maximally about $8 \cdots 10$ (the amount of storage and work grows with 4^L in 2D!). That is no longer true in an adaptive regime, because L could be larger than 20 (in small parts of the domain, for instance near singularities). So, differences of nodal coordinates should not be allowed (except at the beginning).

2.3.2. *Remarks to stable calculation of the Jacobian*

The usual formular for Jacobian inside FE-program structure is

$$T(\hat{g}) = \hat{\nabla} x^T|_{\hat{g}} = \sum_{k=0}^{n-1} \hat{\nabla} N_k(\hat{g})(x^{(k)})^T\,, \tag{3}$$

where $\hat{K}$ is the master element and $\hat{g} \in \hat{K}$. In case of triangle elements, $\hat{K}$ is the unit triangle with vertices $\hat{x}$:

$$\hat{x}^{(0)} = (0,0)^T\,, \quad \hat{x}^{(1)} = e_1 := (1,0)^T \quad \text{and} \quad \hat{x}^{(2)} = e_2 := (0,1)^T\,. \tag{4}$$

$N_0(\hat{x}), \ldots, N_{n-1}(\hat{x})$ are the n form functions defined on $\hat{x} \in \hat{K}$. In the most simple triangular case with $n = 3$, the form functions are

$$N_0(\hat{x}) = 1 - \hat{x}_1 - \hat{x}_2\,, \quad N_1(\hat{x}) = \hat{x}_1\,, \quad N_2(\hat{x}) = \hat{x}_2\,, \tag{5}$$

$\hat{\nabla} = (\partial/\partial\hat{x}_1, \partial/\partial\hat{x}_2)^T$ means formal differentiation with respect to the master coordinates. In the mentioned case

$$\hat{\nabla} N = (-e \,\vdots\, e_1 \,\vdots\, e_2) \tag{6}$$

and

$$T = (x^{(1)} - x^{(0)} \,\vdots\, x^{(2)} - x^{(0)})^T\,. \tag{7}$$

A stable calculation of T and T^{-1} is possible, if we avoid these differences of nodal coordinates in formular (7) for the fine grid elements. If all triangles have got straight edges, the stategy "red-hanging nodes" leads into sub-triangles which are all similar to one of the given coarse mesh triangles.

In that case the Jacobians are $(1/2)T$ (for the son-triangles K_1, K_2 and K_3) and $-(1/2)\,T$ (for K_4), which is totally free of rounding errors.

Other possibilities (green-refinement, quadrilaterals and hexahedrons) are described in Ref. 23. Inside the program structure of AAFEM the stable calculation is just implemented in triangular but not in quadrilateral case.

2.3.3. *The spatial dependence of Young's modulus*

The AAFEM enables input of Young's modulus in two ways:

- **Method 1 — Classical:** In that case the Young's modulus is constant in given coarse elements. Without stable calculation its critical for thin layers like in superlattice coatings. So the simulation of superlattice coatings is realized with the help of the next described method.
- **Method 2 — Scale material:** Definition of $E = E(\mathbf{x})$ with given function (either smooth or jumping). The son-elements will generate the right input Young's modulus, if they are such thin or thinner than the given layer thickness. The adaptive mesh refinement realizes the heaviest stress areas and force refinement there. Examples of input functions are displayed in Fig. 7.

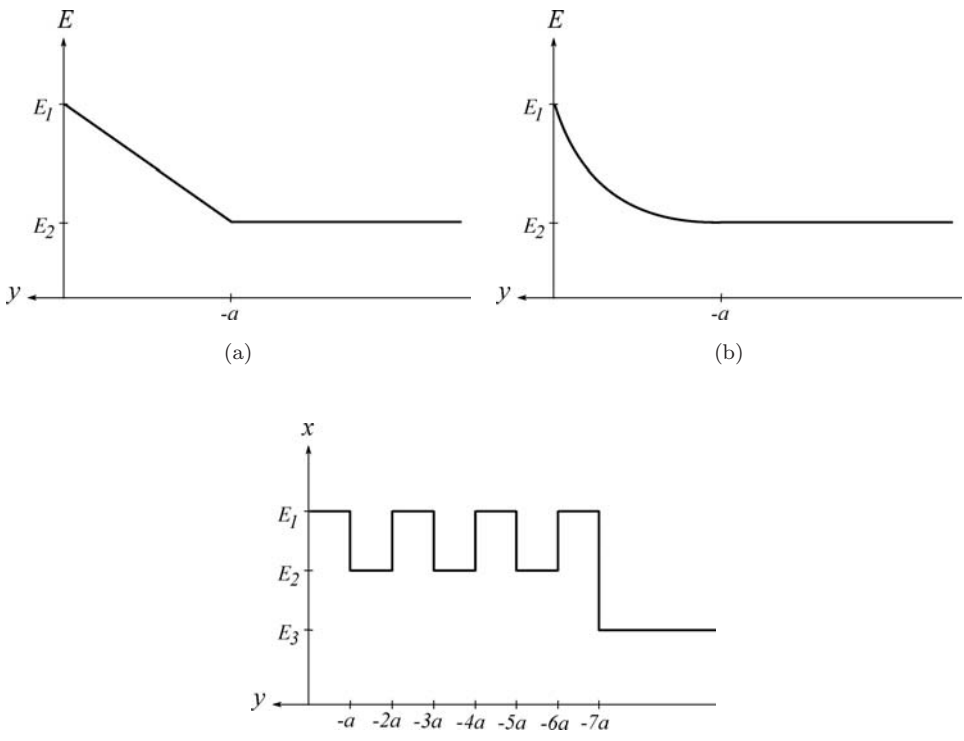

Fig. 7. Possible scale functions (a ... coating thickness, b ... superlattice interval, E ... Young's modulus) — (a) linear function, (b) quadratic function and (c) jumping function.

3. Superlattice Coatings

Referring to the model considered below in Fig. 8 from Ref. 30 (the CPFE is the abbreviation for Crystal Plasticity Finite Element model and EP the abbreviation for elastic plastic model), the modeling structure, used for numerical simulations, is given in Fig. 9. The brinell indenter has rigid boundary conditions. The coating-substrate moves towards the indenter with the help of a force of 500 mN.

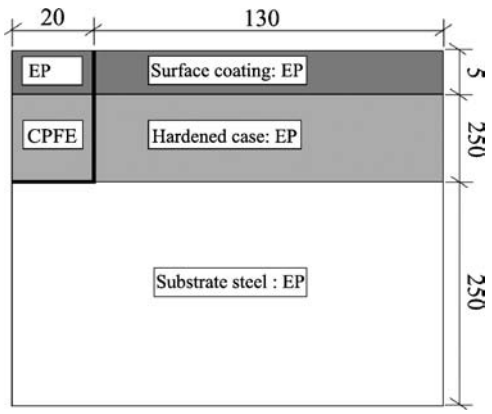

Fig. 8. Modeling structure.

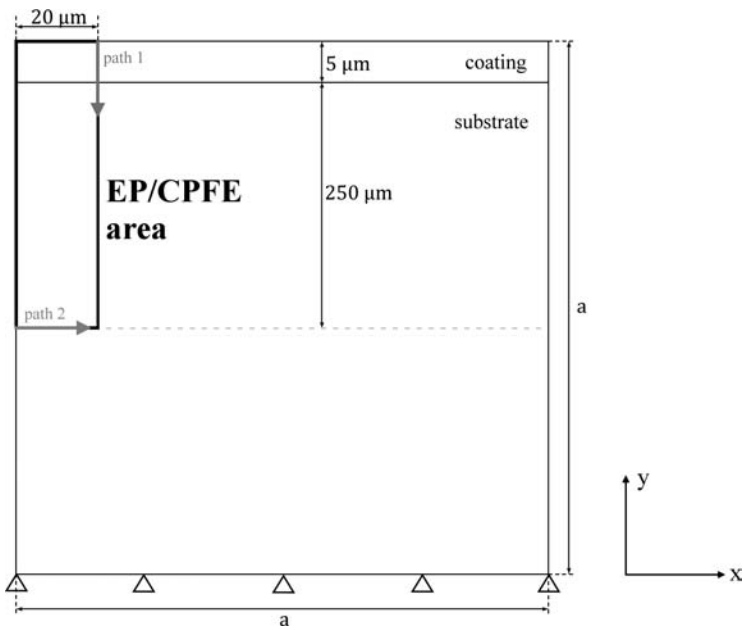

Fig. 9. AAFEM + CPFE-model simulated with EP/CPFE area.

Table 2. Parameter of the model simulated with EP/CPFE-area.

	Material	Width (μm)	Thickness (μm)	Radius (μm)	Young's modulus (GPa)	Poisson's ratio
Indenter		50	50	50	∞	~ 0
Coating	TiN	1000	5		300	0.27
Substrate	Steel	1000	995		220	0.3

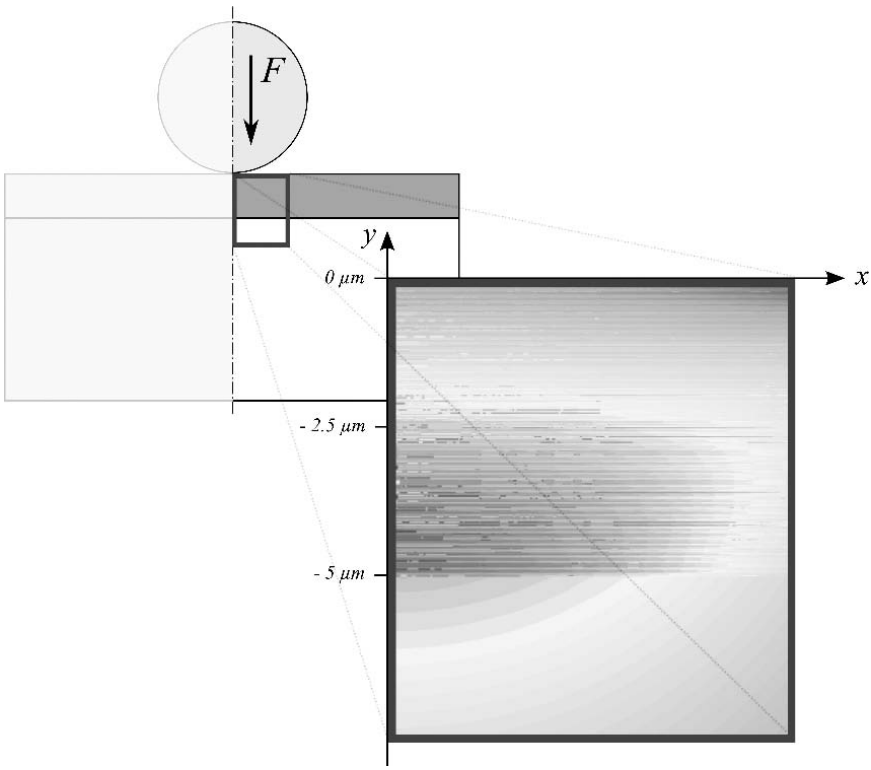

Fig. 10. Layer structure visible with von-mises stress.

In Fig. 9 the measure a can be chosen arbitrary, but for the following calculations $a = 1\,\text{mm}$.

Table 2 contains the material properties of the simulated model.

In this section the AAFEM + CPFE-model above is simulated with a TiN/CrN superlattice coating. The thickness of every layer is 50 nm. It begins with TiN followed by CrN followed by TiN and so on. The different layers are visible within the von-mises stress distribution, given in Fig. 10.

In this way several hundred 50 nm layers are simulated and ended with CrN at transition from coating to substrate.

The material parameter of TiN and steel substrate are the same as in the previous computations. The Young's modulus of CrN lies between 170 MPa and 280 MPa. So three different models are generated:

- Steel substrate with a normal TiN-coating (**Simple TiN-coating**, equal to AAFEM + CPFE-Model seen in Fig. 9) — in this case the model consists of 2,327,764 nodes, 769,385 elements and 2,324,060 edges, the estimated error is at 1.3 E-11
- Steel substrate with a superlattice coating of TiN and CrN that has a Young's modulus of 170 GPa (model **Superlattice-TiNCrN_170**) — in this case the model consists of 3,118,629 nodes, 659,553 elements and 2,156,252 edges, the estimated error is at 8.9 E-11
- Steel substrate with a superlattice coating of TiN and CrN that has a Young's modulus of 280 GPa (model **Superlattice-TiNCrN_280**) — in this case the model consists of 3,280,638 nodes, 1,009,663 elements and 3,177,022 edges, the estimated error is at 2.3 E-11

Table 3 shows the material parameter of the simulated model.

Table 3. Mechanical properties and thicknesses of coatings.

	Material	Width (μm)	Thickness (μm)	Radius (μm)	Young's modulus (GPa)	Poisson's ratio
Indenter		50	50	50	∞	~ 0
Coating	TiN	1000	0.05		300	0.27
	CrN_280	1000	0.05		280	0.27
	CrN_170	1000	0.05		170	0.27
Substrate	Steel	1000	995		220	0.3

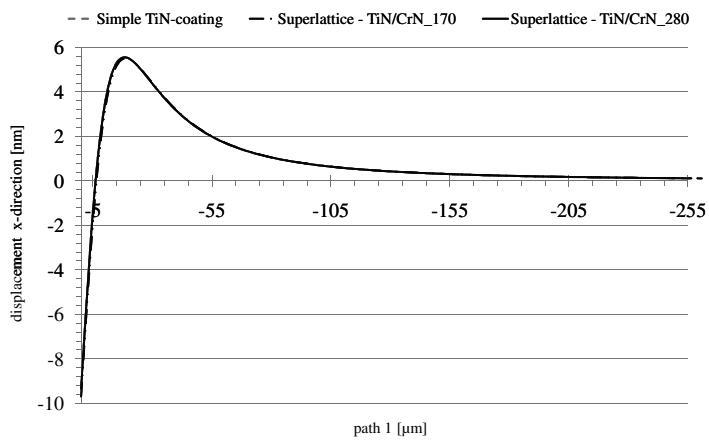

Fig. 11. Displacement in x-direction (nm) along path 1 (μm).

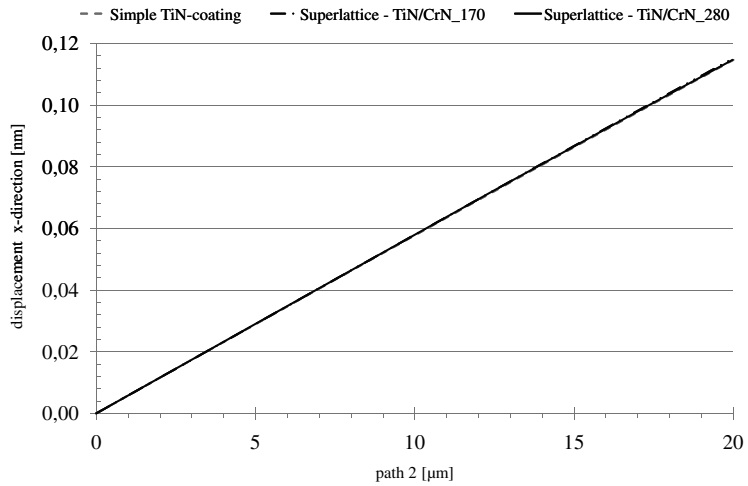

Fig. 12. Displacement in x-direction (nm) along path 2 (μm).

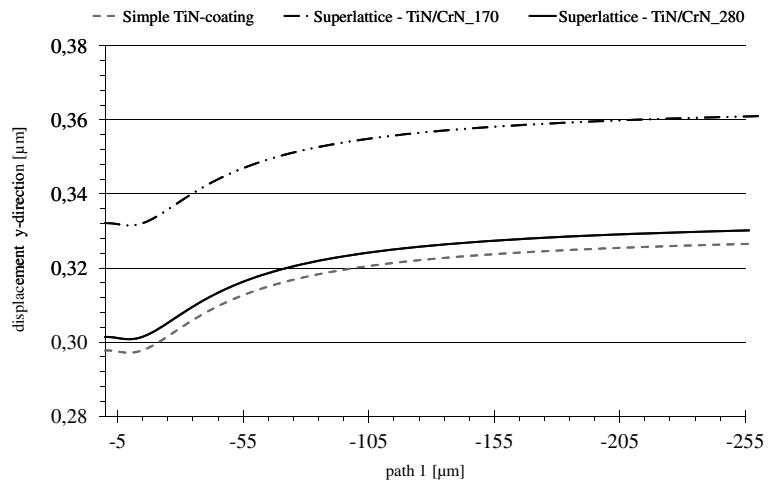

Fig. 13. Displacement in y-direction (nm) along path 1 (μm).

The comparison between the three models, described above (**Superlattice-TiNCrN_280**, **Superlattice-TiNCrN_170** and **Simple TiN-coating**) is recognizable inside the following diagrams. They show the displacement in x- and y-direction along the two paths *path* 1 and *path* 2 defined above.

The displacement in x-direction between the three models is roughly equal. The highest differences are just beween 0 nm and 0.03 nm. However, the displacement in y-direction differs a little more. The simple coating causes the least displacement.

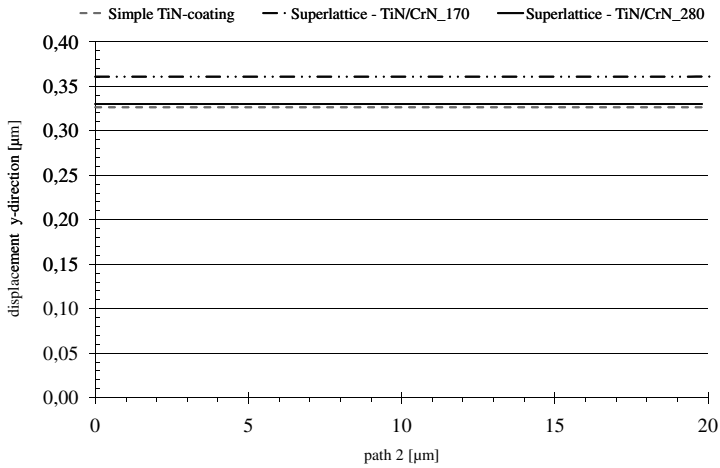

Fig. 14. Displacement in y-direction (nm) along path 2 (μm).

4. Summary

The stability of coating-substrate systems influences the chip formation, the surface integrity of the new generated workpiece surface and above all the productivity of the mechanically manufacturing process.

Using FE simulation, deformations, strains and stresses in coated tools, caused by external and internal loads, can be computed on a microscopic scale. Since both, the whole macroscopic tool (in mm-scale) and the microscopic coating-layers (in μm-scale up to nm-scale) have to be included in the same geometrical simulation model, graded high-resolution FE meshes have to be used. Nevertheless, the number of nodes in a nanoscale computational FE grid reaches some millions, leading to large computational time and storage requirements. For this reason, an AAFEM software has been developed. This philosophy was applied to coating-substrate-simulation of superlattice TiN/CrN-coatings.

Acknowledgment

The authors thank the European Committee for their support on the FP7 project Multiscale Modelling for Multilayered Surface Systems (M3-2S), Grant No: NMP3-SL-2008-213600.

References

1. V. C. Venkatesh, C. T. Ye, D. T. Quinto and D. E. P. Hoy, Performance Studies of Uncoated, CVD-Coated and PVD-Coated Carbides in Turning and Milling, *CIRP Annals — Manuf. Technol.* **40** (1991) 545–550.
2. D. A. Lucca, E. Brinksmeier and G. Goch, Progress in Assessing Surface and Subsurface Integrity, *CIRP Annals — Manuf. Technol.* **47** (1998) 669–693.

3. C. A. van Luttervelt, T. H. C. Childs, I. S. Jawahir, F. Klocke and P. K. Venuvinod, Present situation and future trends in modelling of machining operations progress report of the CIRP working group modelling of machining operations, *CIRP Annals — Manuf. Technol.* **47** (1998) 587–626.
4. R. Kouitat Njiwa and J. von Stebut, Boundary element numerical modelling as a surface engineering tool: Application to very thin coatings, *Surf. Coating. Tech.* **116–119** (1999) 573–579.
5. J. Liebich, J. Schwarte, B. Rau and K.-H. Dittrich, Dry cutting field test with carbon-coated inserts for turning, *NORDTRIB 98: Proc. 8th International Conference on Tribology* (1998).
6. F. Klocke, T. Krieg and K. Gerschwiler, Improved cutting processes with adapted coating systems, *CIRP Annals — Manuf. Technol.* **47** (1998) 65–68.
7. F. Klocke and G. Eisenblätter, Dry cutting, *CIRP Annals — Manuf. Technol.* **46** (1997) 519–526.
8. H. Hollek, Neue Entwicklungen bei PVD-Hartstoffbeschichtungen, *Metall — Internationale Fachzeitschrift* **43** (1989) 7.
9. H. K. Tönshoff and A. Mohlfeld, Increasing interface strength of PVD-coatings by mechanical substrate treatment, *Annals of the German Academic Society for Production Engineering, Production Engineering* **5** (1998) 17–22.
10. Q. Yang, D. Y. Seo and L. R. Zhao, Multilayered coatings with alternate pure Ti and TiN/CrN superlattice, *Surf. Coat. Technol.* **177–178** (2004) 204–208.
11. Q. Yang and L. R. Zhao, Thermal stability of polycrystalline TiN/CrN superlattice coatings, *J. Vacuum Sci. Tech. A* **21** (2003) 558–562.
12. V. C. Lo and W. Jiang, Simulation of stress-induced enhanced dielectric permittivity in ferroelectric superlattice, *Integrated Ferroelectrics* **78** (2006) 35–43.
13. C. D. Wentworth and Y. L. Wang, Monte Carlo simulation study of an ising superlattice structure, *Sol. State Commun.* **74** (1990) 523–527.
14. A. J. Ciani and P. W. Chung, Simulations of dislocations in CdZnTe/SL/Si substrates, *J. Electronic Mater.* **39** (2010) 1063–1069.
15. T. Richter and H. Gläser, Stability analysis of the adhesive strength between substrate and a thin film, *Comput. Mater. Sci.* **9** (1997) 116–120.
16. J. Leopold, M. Meisel, R. Wohlgemuth and J. Liebich, High performance computing of coatingsubstrate systems, *Surf. Coating. Tech.* **142–144** (2001) 916–922.
17. J. Leopold, *High-Performance-Computing of Coating-Substrate-Systems (HPS-CSS)*, CIRP working group 'Modelling of Machining Operations' — STC Cutting. 28th August 1998. Vouliagmeni-Athens/Greece.
18. I. Mircea, Interfacial fracture toughness and adhesion of brittle coatings on ductile substrates, Darmstadt, Darmstadt, TU 2007.
19. F. Q. Tong, W. X. Yu, F. Liu, Y. Zuo and X. Ge, Microstructural study of $BaTiO_3/SrTiO_3$ superlattice, *Mater. Sci. Eng. B* **98** (2003) 6–9.
20. J. Yang, Y. Chen and J. Yan, Molecular dynamics simulation of thermal conductive of superlattice nanowires, *Science in China (Series E)* **46** (2003) 276–286.
21. K. Heller, Numerische Analyse des Kontaktproblems kugelsymmetrischer Indenter auf Schicht-Substrat-Systemen, Diploma thesis. Hochschule Mittweida (FH). University of Applied Sciences, 2010.
22. M. Jung and U. Langer, *Methode der Finiten Elemente fr Ingenieure* (Teubner, Stuttgart 2001).
23. A. Meyer, Stable evaluation of jacobian matrices on highly refined finite element meshes, *Computing* **70** (2003) 359–373.

24. A. Meyer, Basic approach to parallel finite element computations: The DD data splitting, *Lecture Notes in Computational Science and Engineering* **52** (2006) 25–35.
25. A. Meyer, Efficient preconditioners for special situations in finite element computations, *Lecture Notes in Computational Science and Engineering* **52** (2006) 67–85.
26. M. Ainsworth and J. T. Oden, *A Posteriori Error Estimator in Finite Element Analysis* (Wiley, New York, 2000).
27. R. Verfürth, *A Review of a Posteriori Error Estimation and Adaptive Mesh-Refinement Techniques* (Wiley and Teubner, Chichester and Stuttgart 1996).
28. E. Bänsch, Local Mesh Refinement in 2 and 3 dimensions, *IMPACT of Computing in Science and Engineering* **3** (1991) 181–191.
29. A. Meyer, Projection techniques embedded in the PCGM for handling hanging nodes and boundary restrictions, *Engineering Computational Technology* (2002) 147–165.
30. S. Wang, D. Balint and J. Lin, Deliverable 5.2: *Report on methods for the integration of the modelling activities at different scales*, Multiscale modelling for multilayered surface systems, Imperial College, London (2008).